JOURNAL OF MATERIALS SCIENCE 21 (1986) 2297–2307

Microstructural investigation of alpha-beta yttrium sialon materials

C. CHATFIELD, T. EKSTRÖM, M. MIKUS
Research and Development, AB Sandvik Hard Materials, Box 42056, S-126 12 Stockholm, Sweden

Three yttrium sialon materials have been manufactured under similar conditions, but with varying amounts of the constituent phases. Scanning and transmission microscopy, electron probe microanalysis and X-ray diffraction have been used to characterize the microstructure. Precipitation of the alpha-sialon phase both increases significantly the hardness at all temperatures investigated and decreases the thermal diffusivity. The sialon particles frequently contained a core of unreacted Si_3N_4 raw material. This was always found to be alpha-Si_3N_4 in alpha-sialon particles and beta-Si_3N_4 in beta-sialon particles; thus the unreacted Si_3N_4 raw materials act as nuclei for sialon particles.

1. Introduction

One of the very recent trends in the metal cutting field has been the replacement of conventional tungsten carbide cobalt cutting inserts by sialon inserts for the machining of nickel-based alloys used in the aerospace industry. The sialon inserts allow the use of much higher cutting speeds, thus increasing productivity, but provide the same resistance to sudden edge failure as that possessed by the conventional materials.

Sialons are new materials, and considerable research and development effort is directed to both tailor their properties to the specific needs of the metal cutting industry and improve and rationalize production processes. Being constructional materials, the properties of sialons are very dependent upon the amount and properties of the constituent phases [1, 2]. Variables here are the alpha to beta sialon ratio and the amount and composition of the grain-boundary phase. A knowledge of the microstructure is therefore of importance for the understanding of the materials behaviour under different service conditions. In this article are presented the results of an essentially electron-optical investigation of a number of grades to characterize their microstructural differences and to relate them to certain mechanical and physical properties.

2. Materials and experimental procedure

The compositions of the three grades manufactured for this study are given in Table I. The various components are milled in a vibratory mill using Al_2O_3 milling bodies and with propanol as milling fluid. Thereafter, 12 mm × 12 mm × 6 mm cutting inserts were pressed from the dried powder and sintered in nitrogen in a graphite-lined furnace at temperatures in the vicinity of 2000 K. During sintering the specimens were packed in boron nitride powder to reduce loss by evaporation.

After sintering, specimens were prepared for microstructural characterization by grinding and polishing using standard techniques. Specimens for X-ray diffractometry (XRD), scanning electron microscopy (SEM) or electron probe microanalysis (EPMA) were usually studied in this condition or after the application of an evaporated coating of carbon to reduce specimen charging. In certain cases, for example where a mean particle size is needed, specimens were etched in a CF_4 plasma to reveal the grain boundaries between the component phases [3]. Specimens for transmission electron microscopy (TEM) were cut from the inserts, carefully ground to about 50 to 100 μm thickness and then ion-beam thinned to transparency.

The cell parameters of the alpha- and beta-sialon phases vary with their composition and were obtained by XRD in the following manner. The specimen-positioning correction factor was obtained by dusting the specimen surface with a small amount of a standard substance, in this case, TiN with $a = 0.4240$ nm. After using this to correct the position of the diffraction peaks from the alpha- and beta-sialon phases the cell parameters, a and c, of these two hexagonal phases could be obtained using a least-squares programme on a great number of diffraction peaks. The resulting cell parameters are given in Table II.

Finally, the XRD results can be used to give a qualitative estimate of the relative amounts of alpha-sialon, beta-sialon and other phases in the samples. In this case

$$i\,(\%) = \frac{\text{height}_i}{\sum \text{height}_i} \times 100$$

was used and the various values are given in Table II. In this table no account has been taken of the amount of glass phase. An experiment was performed to quantify the measurement of the relative amount of alpha- and beta-sialon. Known volumes of beta-sialon were added to alpha-Si_3N_4, and the relative peak-height ratios, as defined above, were obtained. The data are

0022–2461/86 $03.00 + .12

TABLE I Specimen composition (wt %)

Grade	Si_3N_4	AlN	Al_2O_3	Y_2O_3
1	86	–	8	6
2	83	5	6	6
3	80	8	6	6

shown in Fig. 1. A linear relationship exists between peak-height ratios and volume percentage of beta-sialon added.

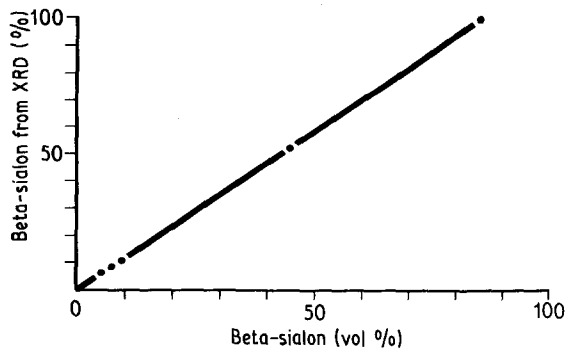

Figure 1 Calibration curve for determining amount of alpha-Sialon in an alpha : beta sialon mixture, using the XRD peak height ratio.

3. Results

3.1. XRD phase analysis

In the text below the following terminology will be used. The alpha-sialon is a phase that has the same structural arrangement of the (Si,Al) $(N,O)_4$ tetrahedra as found for the SiN_4 tetrahedra in alpha-Si_3N_4. The solid-solution phase alpha-sialon is obtained by a substitution of aluminium for silicon, and the overall electronic balance maintained by adding other cations such as yttrium in interstitial positions in the structure. A limited amount of oxygen can also substitute for nitrogen. A general formula for the composition is $M_X(Si,Al)_{12}(N,O)_{16}$ where $X \leqslant 2$ and M is the added cation [4]. In a similar manner the beta-sialon phase has the same atomic arrangement as is found in the beta-Si_3N_4 structure and can be described as a solid-solution series $Si_{6-Z}Al_ZO_ZN_{8-Z}$, where $Z > 0$ and ranges continuously to about $Z = 4$. Neither yttrium nor other cations substitute into the beta-sialon.

X-ray diffractometry revealed that the three materials had rather different phase compositions. Grade 1 contained only one crystalline phase, beta-sialon. In Grades 2 and 3 the major phases were alpha and beta-sialon. All grades could contain small amounts of minor phases. Both Grades 2 and 3 could contain b-phase, "Y_2SiAlO_5N", having an alpha-wollastonite type of structure. Grade 3 also contained minor amounts of the 12H sialon polytype. A summary of the phase analysis of these grades is given in Table II.

From a knowledge of beta-sialon cell parameters it is possible to obtain a value for Z in the formula $Si_{6-Z}Al_ZO_ZN_{8-Z}$ by assuming that it is a linear function of the shift of the a- and c-axes of the hexagonal unit cell. At $Z = 0$ and $Z = 4$ the corresponding cell parameters were set to $a = 0.7603$ nm, $c = 0.2909$ nm and $a = 0.7716$ nm, and $c = 0.3004$ nm, respectively. The accuracy of the evaluation method as such is estimated to lie within ± 0.05 in the Z value. However, it must be stressed that this only gives an overall mean composition for the diffracted crystals. The Z values obtained are given in Table II.

According to Hampshire *et al.* [4] it is also possible to determine the composition of alpha-sialon from measured cell parameters. They have suggested for a general alpha-sialon composition the formula

$$M_XSi_{12-(m+n)}Al_{(m+n)}O_nN_{16-n}$$

and have shown that cell parameters can be obtained from a knowledge of m and n by the following two relationships:

$$\Delta a\ (\text{nm}) = 0.0045\ m + 0.0009\ n$$

$$\Delta c\ (\text{nm}) = 0.004\ m + 0.0008\ n$$

where the cell parameters of alpha-Si_3N_4 are $a = 0.776$ nm and $c = 0.562$ nm. However, we find that the cell parameters obtained for the alpha-sialon formed in Grades 2 and 3 cannot be described by the above relationship. The c cell parameter always has a much larger value for $(m + n)$ than is required for the a cell parameter. This observation is also supported by the alpha-sialon cell parameters of $a = 0.78293$ nm and $c = 0.57076$ nm for the composition. $Y_{0.5}Si_{9.3}Al_{2.7}O_{0.9}N_{15.1}$ recently reported by Izumi *et al.* [5]. Because of this uncertainty in the effect of composition upon cell parameters they can only be used to suggest an approximate composition of $Y_{0.3}Si_{10.2}Al_{1.8}O_{1.2}N_{14.8}$ for the alpha-sialon in Grades 2 and 3.

3.2. Microstructural analysis

The morphology of the two major phases, alpha-sialon and beta-sialon, is revealed in the micrographs in Fig. 2. In these micrographs, taken from unetched but carbon-coated surfaces, the various phases are easily revealed by their atomic-number contrast which is dependent upon their yttrium content. In Fig. 2 the alpha-sialon is light-grey, beta-sialon (which contains no yttrium) is dark grey and the glass/b-phase is very bright. From these micrographs it would appear that

TABLE II Results of XRD investigation: phase analysis of the crystalline phases present and the lattice parameters of the sialon phases

Grade	Estimated amounts (%)				Lattice parameters (nm)				Z value of beta-sialon
	Alpha	Beta	b phase	12H	Alpha		Beta		
					a	c	a	c	
1	0	100	0	0	–	–	0.7610	0.2913	0.22
2	27	70	3	0	0.7801	0.5679	0.7622	0.2921	0.60
3	34	56	8	2	0.7803	0.5684	0.7624	0.2923	0.68

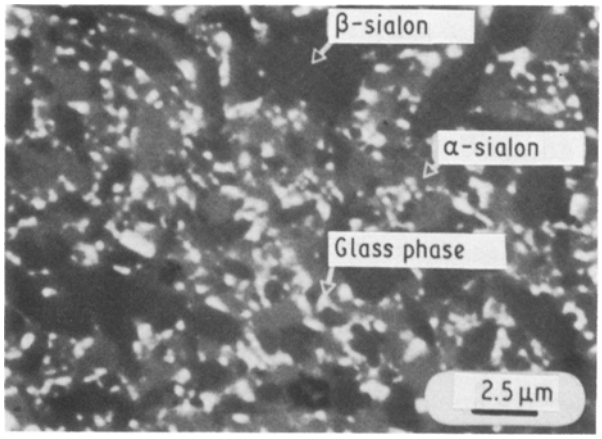

Figure 2 SEM photomicrograph of unetched but carbon-coated Grade 2, illustrating the contrast difference between the component phases. Micrograph is taken using the secondary electron (SE) detector.

some of the beta-sialon particles are very large. The existence of similar large alpha-sialon particles is rare. These micrographs indicate a binomial particle-size distribution for the beta-sialon.

To delineate grain boundaries between particles it is necessary to plasma-etch the specimens. From the photomicrographs shown in Fig. 3 it is very easy to measure a mean sialon particle size, but as the atomic-number contrast is now submerged by the secondary electron contrast, it is not possible to separate alpha-sialon from beta-sialon and measure their respective mean grain sizes. The mean sialon particle sizes were 1.3 μm for Grade 1 and 1.5 μm for Grades 2 and 3. From the micrographs in Fig. 3 it appears that the sialon particles are either plates or rods. By etching specimens in molten alkali carbonate it was possible to show that the reaction-sintered sialon particles are rods with a hexagonal cross-section (Fig. 4).

Plasma-etching also reveals that many sialon grains contain an internal structure (Figs. 5a and b). The cores in the rods were shown by EPMA to be unreacted Si_3N_4 and in turn each core was surrounded by an aluminium-rich border (Fig. 5c).

These features were examined in more detail in the TEM. Cores in alpha-sialon and beta-sialon grains are shown in Fig. 6. Each core is generally surrounded by a heavily dislocated region, the boundary between the core and the rod proper being some form of low-angle boundary. In all cases it was found that a beta-sialon rod had a beta-Si_3N_4 core and an alpha-sialon rod had an alpha-Si_3N_4 core.

In the region surrounding the cores other phases could also be found. These seemed to be of two types: non-crystalline and crystalline particles. The former showed no diffraction contrast upon tilting the rod, and energy-dispersive spectrometry (EDS) showed that they contained yttrium and aluminium (and silicon), i.e. they are probably particles of glass phase trapped in the alpha- or beta-sialon rods during their growth. The crystalline particles were composed of silicon, but their identity was not determined. EDS analysis of the beta-sialon rods in the vicinity of the cores also showed that they contained much more aluminium than expected from their overall composition, and that this was not due to the glass inclusions.

In Grades 1 and 2 the material between the sialon rods was a glass (Fig. 7). In Grade 3 only a crystalline phase, b-phase, was observed (Fig. 8). In this case the b-phase particles are larger than the mean free path between the silicon-nitride based phase. As XRD had shown that Grade 2 should contain about 3% b-phase, the failure to observe any b-phase is hard to understand unless crystallization has only occurred at a few places throughout the material.

All grades contained minor amounts of other phases. Some of these originate from impurities in the starting materials. For instance, small amounts of iron are sometimes added to facilitate the production of silicon nitride from silicon [6]. However, the iron content of the silicon nitride used to manufacture Grades 1 to 3 was very low and the amount of iron silicides, the phase normally formed in the presence of iron impurities, was subsequently very small. Fig. 9 illustrates an iron silicide/SiC complex observed in Grade 2. The iron silicide has a distorted NaCl crystal structure (a = 0.446 nm) and is heavily alloyed with trace elements (Table III). Adjacent to this particle and in contact with it are nucleated SiC-based crystals. Crystal A in Fig. 9 is beta-SiC, whilst Crystal B is a beta-SiC polytype with one cell parameter of about

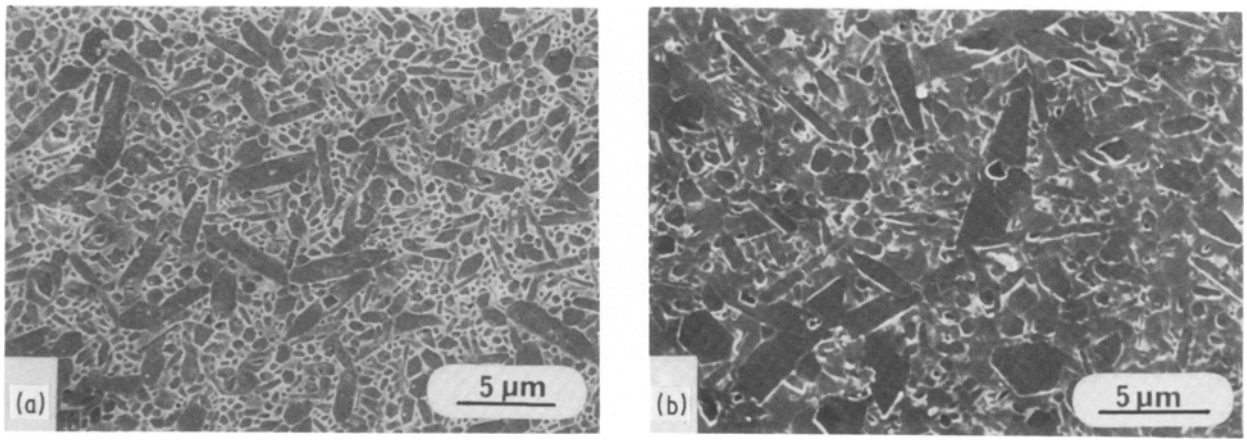

Figure 3 SEM photomicrographs of plasma-etched materials (a) Grade 1, (b) Grade 3. Grade 1 has been etched for a longer time than Grade 3.

TABLE III Composition of iron silicides from semi-quantitative EDS (at %)

Particle	Si	Fe	Co	Mn	Ti	Al	Y
1	64.2	26.1	0.7	1.6	7.4	0	0
2	61.2	16.8	0.5	1.0	0.8	7.5	12.3
3	57.4	25.4	1.4	1.6	2.2	11.3	0.8
4	52.2	16.3	0.1	0.8	0.2	6.5	23.9

1.7 nm. These iron silicide/SiC complexes are visible on unetched sections under the optical microscope. Grade 3 also contained aggregates of a 12H sialon polytype phase [7, 8] (Fig. 10). In the bright-field image the (0 0 0 1) planes, which have an interplanar spacing of about 3.4 nm, are readily visible.

The presence of the sialon polytypes was not easy to determine in scanning electron micrographs, as it exhibits a medium-grey contrast similar to that of the alpha-sialon phase. However, using the cathodoluminescence detector attached to the EPMA and set to image total emitted light from the specimen, the sialon polytypes could be readily distinguished from the other phases (Fig. 11). These polytypes can also be detected by using the EPMA to map the local variations in aluminium. Grade 3 was estimated to contain no more than 5% polytype by this method. As already noted, this 12H polytype was detected by XRD. However, as expected from the heavy faulting seen in the TEM photomicrographs, considerable peak broadening had occurred resulting in rather weak peaks. The XRD method for obtaining the phase composition will probably underestimate the amount of 12H polytype in such cases.

3.3. Phase composition

The composition of the component phases, e.g. alpha-sialon, beta-sialon, 12H sialon polytype and glass/b-phase, were measured using EPMA and EDS. In the case of EPMA measurements the specimen itself was used as a standard. The composition of the various phases, in wt %, as measured using the EPMA are given in Table IV. The compositions of the beta-sialon phase as determined by EPMA are in good agreement with the approximate compositions determined by XRD and also given in Table IV. Notice that while the composition of the beta-sialon in the three specimens changes, the composition of alpha-sialon is virtually constant in agreement with the XRD results. Also the alpha- and beta-sialon phases were sufficiently coarse-grained for no difficulty to be experienced in measuring their composition using the EPMA.

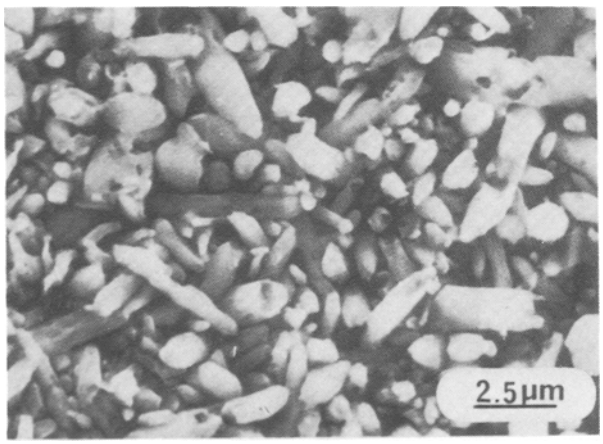

Figure 4 SEM photomicrograph of Grade 1 after etching in molten alkali carbonate. The beta-sialon particles are long rods with a hexagonal cross-section.

The 12H sialon polytype falls on the line connecting the AlN and SiO_2 phases in the Si_3N_4–SiO_2–AlN–Al_2O_3 phase diagram. Its composition may be written as 5AlN:1SiO_2 or $Si_{0.08}Al_{0.38}O_{0.15}N_{0.38}$. However, it is well known that the sialon polytypes have extended solubility ranges [1]. The composition of the 12H sialon in Grade 3 is about $Y_{0.006}Si_{0.16}Al_{0.34}O_{0.11}N_{0.39}$, which indicates that it falls at the silicon-rich end of such a solid-solution range.

The glass/b-phase areas in all grades are small, and due to beam spreading it is difficult to obtain a correct analysis for these areas using EPMA. They are expected to have too high a silicon content. Thus the glass/b-phase in all three grades was analysed using the EDS equipment in the TEM. These results are given in Table V. Note that they are only semi-quantitative. However, the relative difference between grades is correct. Also given in Table V are the EPMA results after conversion to atomic percentages and normalization to 100% metallic constituents. Comparing EDS and EPMA results it appears that, as expected, the EPMA results indicate a much higher silicon content than the EDS results. However, both methods for measuring composition are in agreement in that on going from Grades 1 to 2 the aluminium content decreases and the yttrium content increases in the glass/b-phase. The compositional differences in this phase between Grades 2 and 3 are not significant.

It was also found that the EPMA results could be corrected for beam spreading. First the silicon content was reduced to that of the EDS results, and the aluminium and yttrium results increased in proportion to give once more 100% of metallic constituents. These corrected results are also given in Table V. The EDS results are now identical with the corrected EPMA results. This indicates that despite being semi-quantitative the composition of the glass/b-phase as determined by EDS analysis is close to the true analysis. Alternatively, EPMA analysis of the glass phase can be used to qualitatively study changes in glass/b-phase composition. Unfortunately neither method can indicate the true amount of oxygen and nitrogen in the glass/b-phase.

3.4. Properties

The properties of interest for metal-cutting inserts are toughness and hardness, particularly at elevated temperature, and thermal diffusivity. Lack of sufficient toughness leads to the cutting inserts being susceptible

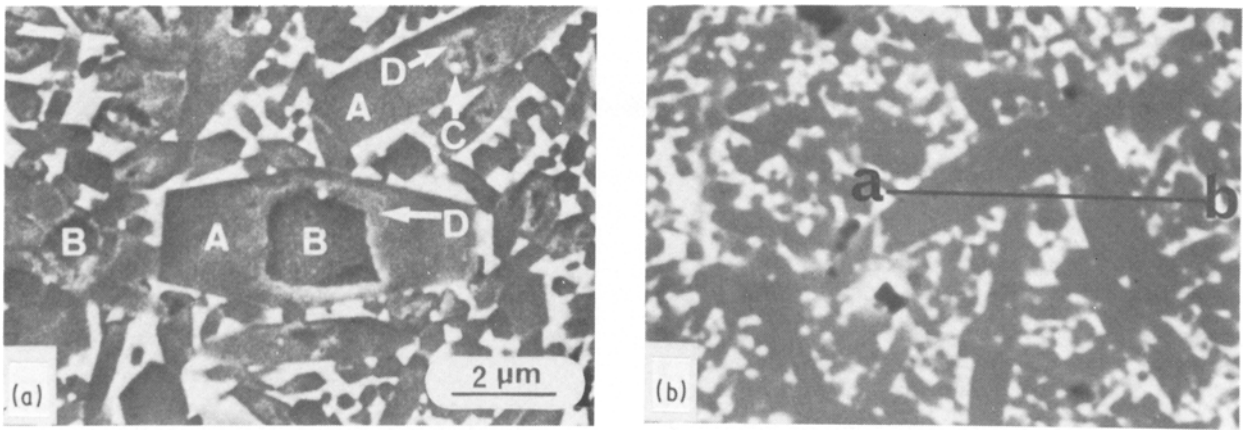

Figure 5 Cores in Sialon particles: (a, b) plasma-etched specimen, A = beta-Sialon, B = Si_3N_4, C = entrapped glass particle, D = aluminium-enriched beta-Sialon; (c) EPMA X-ray line scan across beta-Sialon particles from a to b in (b). The Si_3N_4 cores are surrounded by aluminium-enriched beta-Sialon.

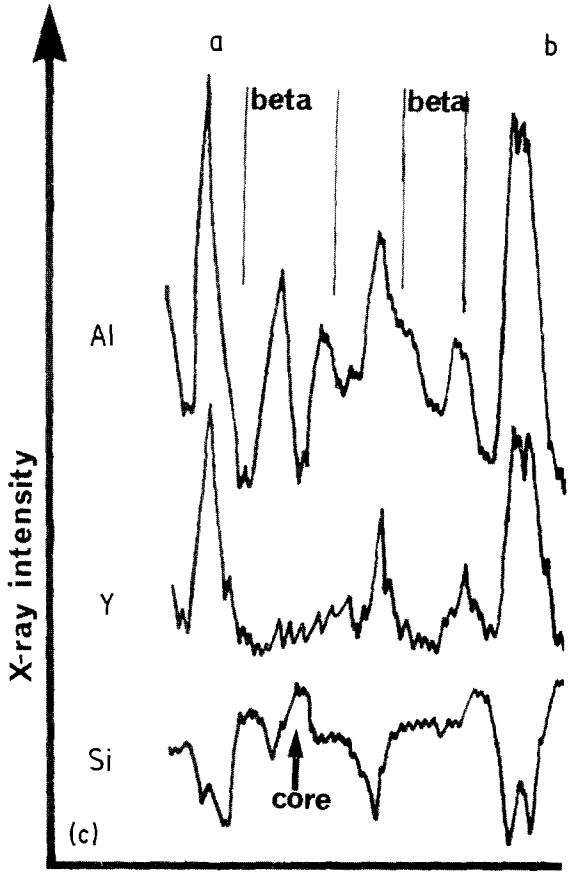

to gross insert failure due to sudden overload, or to small-scale edge-chipping under more usual cutting conditions. The toughness requirements become more stringent for operations in which mechanical or thermal cycling occurs, e.g. in milling. Other types of insert failure can be the result of excessive plastic deformation due to too low a tool hardness. Thermal diffusivity controls the flux of heat in the insert from the region of contact between the cutting insert and the workpiece. The temperature existing in this region is of great importance for tool performance as it controls both the rate of chemical wear [9] and the amount of plastic deformation that occurs.

Hardness was measured using a load of 98.1 N (HV_{10}). At the same time the identation fracture toughness of the three grades was calculated using the method of Anstis *et al.* [10] after measuring the total length of the cracks emanating from the corners of the hardness impressions. Young's modulus, E, was assumed to be 300 GPa. Both hardness and indentation fracture toughness values are given in Table VI.

TABLE IV Composition of phases in the three grades

Grade	Phase	Composition (wt %)				
		Si	Al	Y	O	N
EPMA results						
1	Beta	58.0 ± 0.6	2.6 ± 0.3	0	1.3 ± 0.2	36.2 ± 0.7
	Glass	32.7 ± 4.8	9.2 ± 1.2	20.9 ± 3.4	25.2 ± 3.8	17.3 ± 4.1
2	Alpha	47.9 ± 1.1	7.6 ± 0.5	4.4 ± 0.6	3.2 ± 0.2	36.4 ± 2.3
	Beta	52.8 ± 1.7	5.3 ± 1.4	0	3.2 ± 0.8	36.2 ± 1.7
	Glass	31.0 ± 2.8	6.2 ± 2.8	29.4 ± 0.6	16.1 ± 1.4	28.0 ± 1.1
3	Alpha	47.8 ± 1.0	8.3 ± 0.9	4.7 ± 0.6	3.6 ± 0.4	36.7 ± 2.5
	Beta	52.5 ± 0.9	5.9 ± 0.9	0	3.3 ± 0.6	34.0 ± 2.9
	Glass	32.0 ± 0.6	6.1 ± 0.9	30.8 ± 3.4	15.9 ± 2.8	30.7 ± 3.4
	12H	21.0 ± 0.8	40.6 ± 1.4	3.4 ± 1.2	8.9 ± 0.6	26.1 ± 2.9
XRD results (for beta-sialon only)						
1	Beta	57.8	2.1	0	1.3	38.8
2	Beta	53.9	5.8	0	3.4	36.9
3	Beta	53.1	6.5	0	3.9	36.5

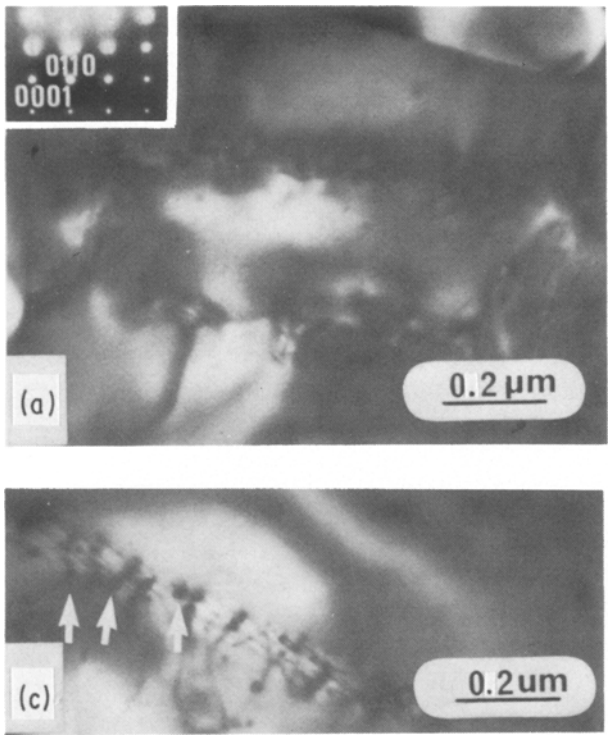

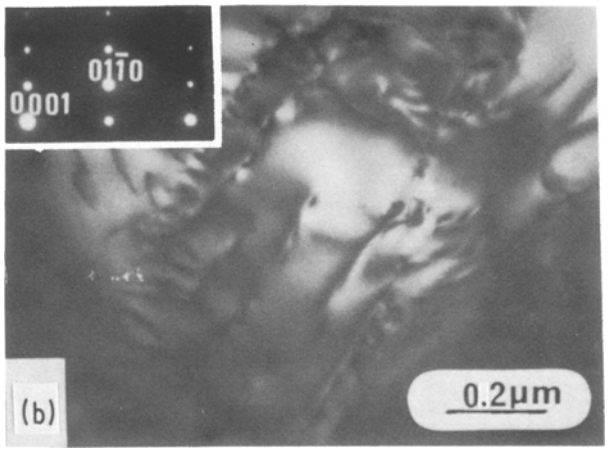

Figure 6 TEM photomicrographs of cores in Sialon particles: (a) alpha-Sialon particle, [2 $\bar{1}$ $\bar{1}$ 0] orientation; (b) beta-Sialon particle, [2 $\bar{1}$ $\bar{1}$ 0] orientation; (c) illustrating the interface between core and particle. Note interfacial dislocations and glass-phase particles at the interface. In all micrographs dislocations can be seen spreading out in the particle.

The variation of the hardness of the three grades with temperature is shown in Fig. 12. The hot-hardness of Grade 1 is much less than that of Grades 2 and 3. The thermal diffusivity of Grades 1 and 3 was measured using the laser-flash method [11] and the results are plotted in Fig. 13. Grade 3 has initially a much lower diffusivity than Grade 1, but the relative difference decreases with increasing temperature.

4. Discussion

Pressureless sintering of dense Si_3N_4 materials always involves a liquid phase during the densifying step. In the present samples the addition of 6% Y_2O_3 and some Al_2O_3 are the most important sintering aids. During the sintering process these oxides form a liquid phase, together with the SiO_2 on the surface of the Si_3N_4 grains and some dissolved Si_3N_4 [12, 13]. This liquid occupies a considerable volume of the body and plays an important role in the growth of the beta- or alpha-sialon phases, often, as found here, on nuclei of undissolved Si_3N_4 crystallites. Depending upon the overall composition and the rate of cooling from the sintering temperature, a glass phase will remain in the microstructure. The materials properties, especially high-temperature mechanical properties, will be greatly influenced by the amount, distribution and composition of this glass phase.

Other crystalline phases than Si_3N_4-related phases might also form from the liquid phase, if it has the appropriate composition, either during a controlled sintering/cooling process or during a post-sintering annealing. It is believed that a low remaining glass content in a sialon material will favour high-temperature strength, but it is not universally true that a reduction of glass content will favour the properties of a sialon material in service as a cutting tool. As an example it can be said that Grade 1 contains about 15% of glass, has a good toughness, and performs very well as a cutting tool material in turning cast iron. Post-heat treatment at temperatures above 1400 K causes the glass to partially recrystallize into the yttrium–aluminium–garnet, $3Y_2O_3 \cdot 5Al_2O_3$ (YAG). The toughness of the material decreases and the cutting-tool performance in turning cast iron drops drastically.

The three sialon compositions studied here contain a constant weight percentage of Y_2O_3, but increasing amounts of AlN (Table I). Grade 1 is a two-phase beta-sialon + glass mixture. Increasing the AlN + Al_2O_3 content results in the precipitation of alpha-sialon. A further increase in AlN and Al_2O_3 increases the amount of alpha-sialon in the specimens and results in the precipitation of a sialon polytype. Changes also occur in the composition of the individual phases. There is an increase in the Z parameter, i.e. the amount of aluminium and oxygen in solution,

TABLE V Glass phase compositions (at %)

Grade	Si	Al	Y
EDS results			
1	46.2	32.9	21.0
2	37.9	24.0	38.2
3	37.2	23.4	39.4
EPMA results (metallic constituents)			
1	66.8	19.6	13.6
2	66.3	13.8	19.9
3	66.6	13.1	20.3
EPMA results, corrected for silicon			
1	46	32	22
2	38	25	37
3	37	25	38

TABLE VI Room-temperature hardness and K_I^{IDT} values

Grade	Hardness (HV_{10})	K_I^{IDT} (MPa $m^{1/2}$)
1	1460	4.4
2	1700	4.1
3	1760	3.7

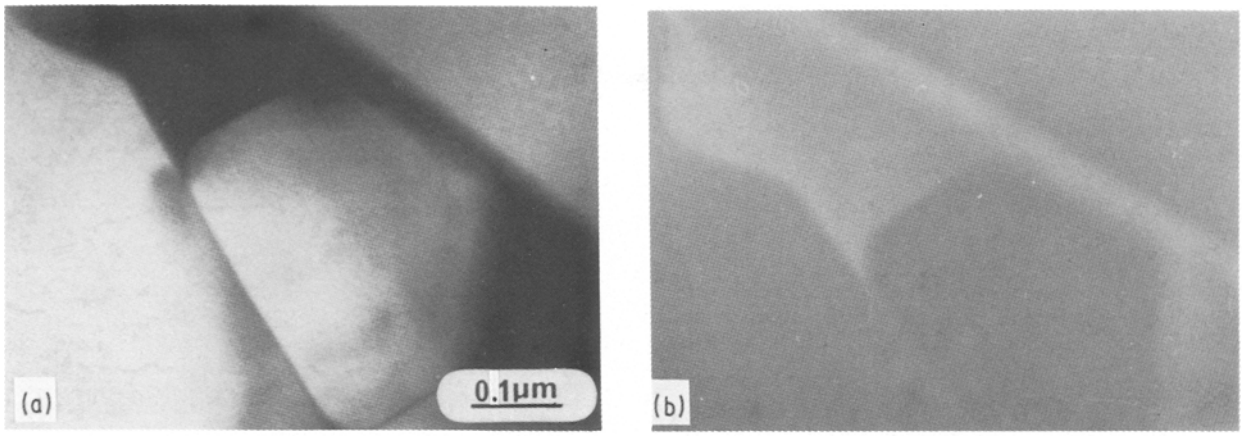

Figure 7 Glass-phase pockets existed in Grades 1 and 2: (a) Grade 2 bright-field photomicrograph; (b) dark-field micrograph of same area imaged using amorphous ring.

in the beta-sialon. The composition of the alpha-sialon, however, appears to remain constant.

These results are in qualitative agreement with the phase relationship diagram for the alpha-sialon plane recently presented by Spacie *et al.* [14] (Fig. 14a). However, there are some small discrepancies between this diagram and our results which will now be discussed.

Firstly, both the XRD and EPMA results indicate that the alpha-sialon in Grades 2 and 3 has a composition that lies slightly outside the range of existence of alpha-sialon suggested by Jack and co-workers [4, 15] and Spacie *et al.* [14]. It also does not appear to lie in the alpha-sialon plane of the phase relationship diagram. The approximate composition suggested by XRD is $Y_{0.3}Si_{10.2}Al_{1.8}O_{1.2}N_{14.8}$. The corresponding composition obtained from the mean of the EPMA results in Table IV and adjusted to give (Si + Al) = 12 is

$$Y_{0.3\pm0.1}Si_{10.2\pm0.4}Al_{1.8\pm0.1}O_{1.3\pm0.1}N_{15.7\pm0.5}$$

and this is considered a more accurate description of the composition of the alpha-sialon. The uncertainties in the composition have been approximated from the standard deviations given in Table IV. An alpha-sialon lying in the alpha-sialon plane in the phase relationship diagram and having a composition close to that suggested for Grades 2 and 3 in our study would be

$$Y_{0.3}Si_{10.2}Al_{1.8}O_{0.9}N_{15.1}$$

Taking into account experimental errors, the difference in composition, especially oxygen content, is sufficiently great to confirm that the composition suggested for alpha-sialon in Grades 2 and 3 is different from that of one lying in the alpha-sialon plane.

Thus as one moves from the ternary Si_3N_4–Al_4N_4–Y_4N_4 phase diagram by making additions of oxygen, the alpha-sialon phase field opens up to include compositions out of the plane defined by the ternary alpha-sialon.

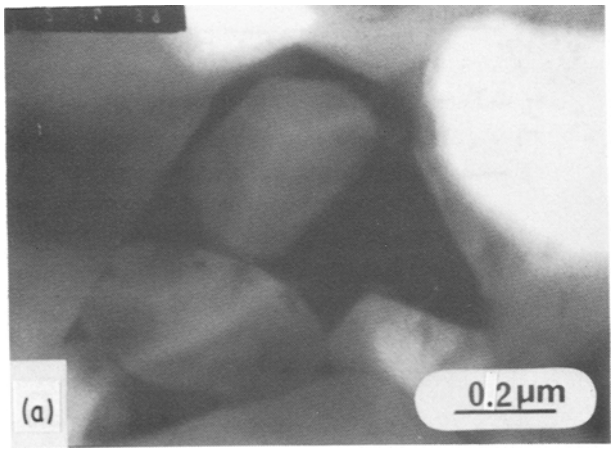

Figure 8 b-phase (Y, $SiAlO_3N$) in Grade 3: (a) bright-field micrograph; (b) dark-field micrograph imaged using (1 $\bar{1}$ 0 0) reflection; (c) [2 $\bar{1}$ $\bar{1}$ 3] diffraction pattern of b-phase.

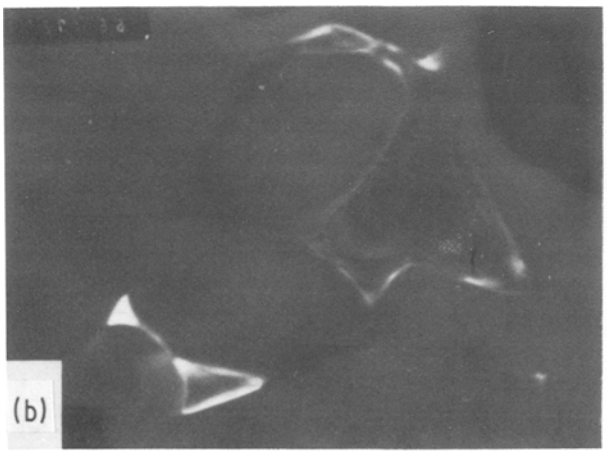

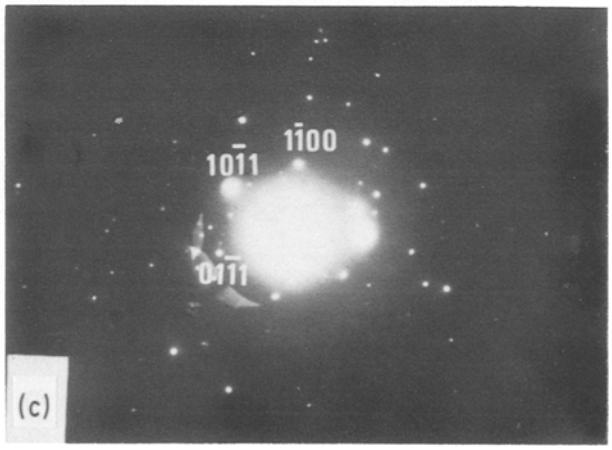

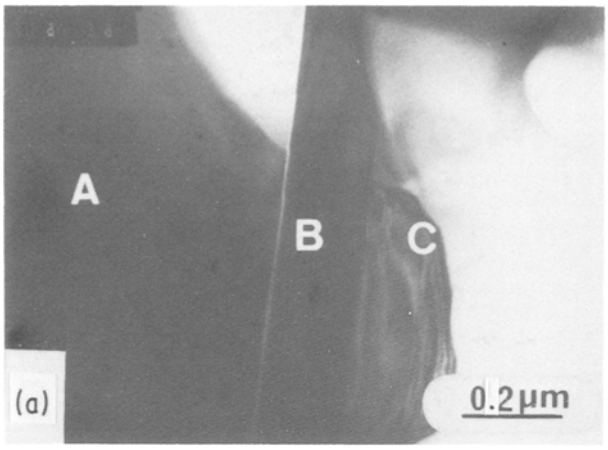

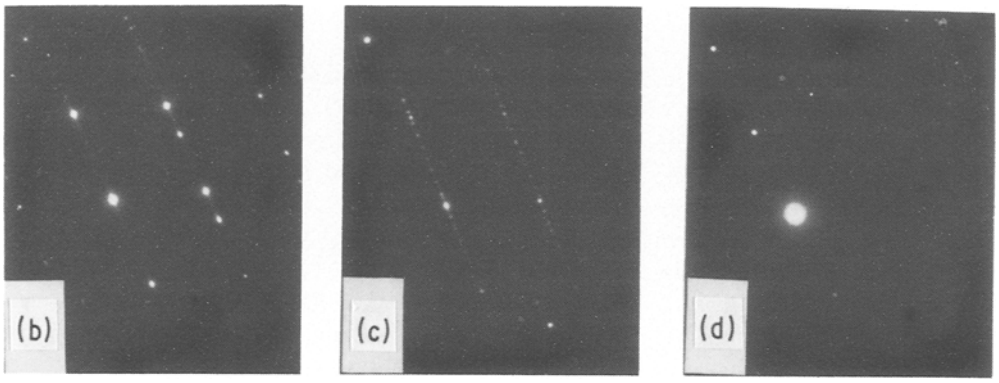

Figure 9 TEM photomicrograph of an FeSi/SiC complex: (a) bright-field micrograph of complex, A = FeSi, B = SiC polytype, C = twinned beta-SiC; (b) [$\bar{1}\,\bar{1}\,0$] diffraction pattern from beta-SiC; (c) diffraction pattern from SiC polytype; (d) [2 3 5] diffraction pattern from FeSi.

Secondly, both the alpha- and beta-sialons in Grades 2 and 3 have compositions very close to one another. Grade 2 lies in the three-phase field (alpha + beta + glass), whilst Grade 3 lies in the four-phase field (alpha + beta + glass + 12H). By making the assumption that at the sintering temperature, which is about 2000 K, the extent of the alpha-sialon phase field out of the ternary alpha-sialon phase is not large, it is possible to sketch a phase-relationship diagram in the vicinity of the Si_3N_4 corner. This is shown in Fig. 14b. The extent of the alpha-sialon phase field along the Si_3N_4–YAl_3N_4 line has been calculated from the formula given by Spacie *et al.* [14]

$$Y_{y/3}Si_{12-y}Al_yN_{16} \qquad y = 1.2 \text{ to } 3.4$$

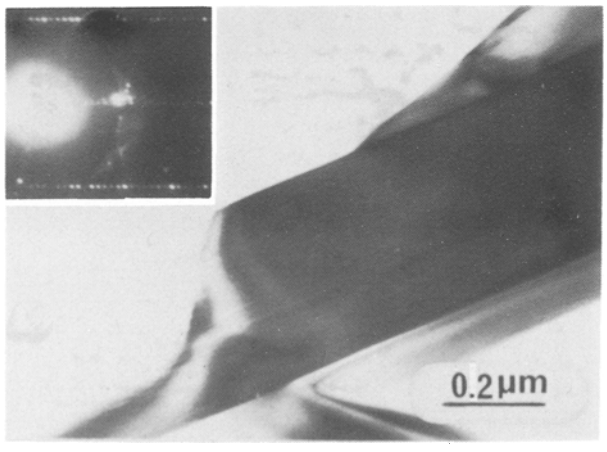

Figure 10 12H Sialon polytype oriented so that [1 1 $\bar{2}$ 0] is parallel to beam direction.

Also plotted are the compositions of the oxygen-containing alpha-sialons manufactured by Hampshire *et al.* [4] at 2020 K and Huang *et al.* [16] at 1970 to 2020 K.

The main difference between the incomplete phase relationship diagram in Fig. 14b and that of Spacie *et al.* [14] in Fig. 14a is the direction of the boundary separating the phase field (alpha + beta) from the phase field (alpha + beta + 12H + liquid). In our case this boundary slopes towards the Si_3N_4 corner, whilst that of Spacie *et al.* points away from Si_3N_4. The phase-relationship diagram suggested by us is very similar to that suggested by Jack [17] for the alpha-sialon plane in the Si_3N_4–$Al_4O_4N_{4/3}$–$Ca_{1.5}Al_3N_4$ phase-relationship diagram.

Large changes in glass phase composition also occur upon going from Grade 1 to Grades 2 and 3. The yttrium content of the glass phase greatly increases. Yttrium is soluble in both alpha-sialon and the glass phase. Thus to maintain a mass balance this means that the amount of glass phase in Grades 2 and 3 has decreased quite considerably. In addition, the glass phase will contain more nitrogen.

The changes in the relative proportions of the various phases and their compositions will clearly influence both the sintering behaviour of the materials and their properties. For instance, an increase in the yttrium content or nitrogen content of the glass is expected to increase its viscosity [18] and thus make the attainment of full density during sintering more difficult. This will be compounded if the amount of glass decreases simultaneously. Indeed, in agreement with this argument both Grades 2 and 3 were more

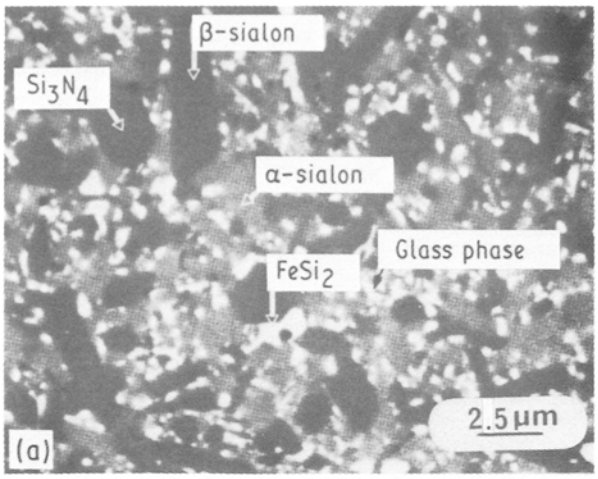

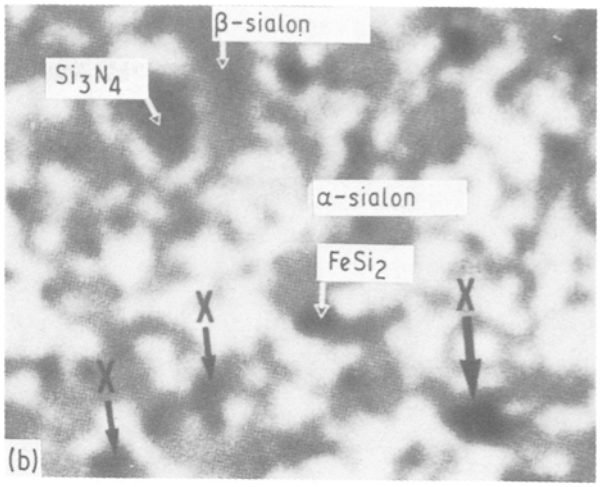

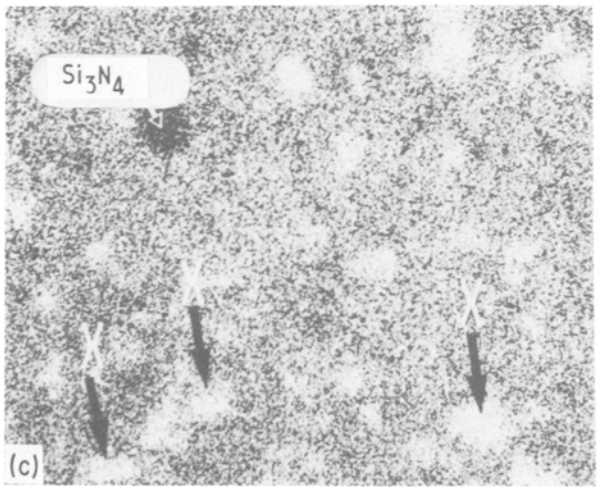

Figure 11 Detection of the 12H Sialon polytype with the EPMA: (a) SEM micrograph of Grade 3; (b) cathodoluminescence micrograph with detector set to image total emitted light; (c) aluminium X-ray map of same area. The 12H Sialon particles are marked X.

difficult to sinter to full density than Grade 1. Despite the similarity in the cation contents of the glass phase in Grades 2 and 3, the differences in their recrystallization behaviour indicate that they probably have different anion contents.

The varying phase content of these specimens has large effects upon their hardness, especially at elevated temperatures. Alpha-Si_3N_4 has a higher hardness than beta-Si_3N_4 [19] and, as expected, the alpha- and beta-sialon mixtures have both a higher room-temperature hardness and higher elevated-temperature hardness than beta-sialon alone. Hardness appears to increase in proportion to the amount of alpha-sialon. Factors not taken into account here are the reduction in the amount of glass phase and changes in its composition. According to Hampshire *et al.* [18], Y–Si–Al–O–N glasses with a cation content of 25.5 Y, 45.5 Si, 29 Al and varying anion contents had hardness ($HV_{0.1}$) in the range 900 to 970. Thus any reduction in glass phase will result in a higher hardness. The hardness difference between Grades 1 and 2 is too great, however, to be due to a reduction in the amount of glass phase alone.

As fracture toughness, K_I^{IDT}, is inversely related to hardness then Grades 2 and 3 are expected to be less tough than Grade 1, as is the case. The toughness values also indicate that the change from a partially crystallized to a possibly fully crystallized glass phase does not result in any great loss of toughness at small amounts of glass phase. It is well known that sialons undergo a drastic loss in transverse rupture strength when the glass phase becomes sufficiently soft [20]. The temperature range over which this occurs has not been investigated in this study, because such temperatures cannot be achieved in the hot-hardness tester. However, Grades 2 and 3 are intuitively expected to resist "softening" better at high temperatures because of their high-yttrium, partially crystalline glass phase.

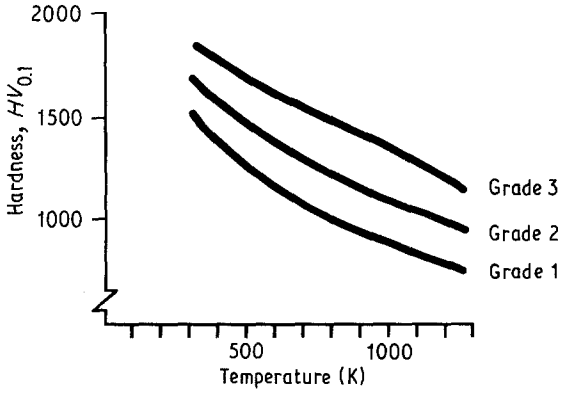

Figure 12 Variation of hardness of Grades 1, 2 and 3 with temperature.

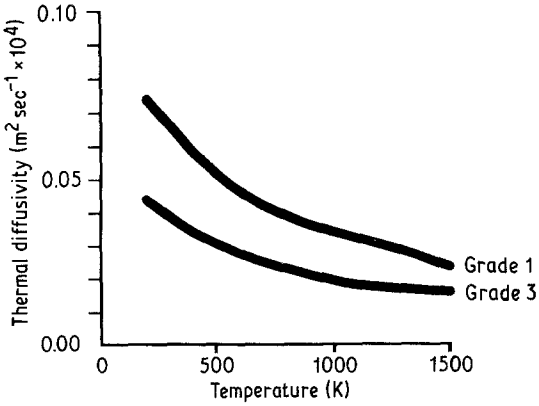

Figure 13 Thermal diffusivity of Grades 1 and 3.

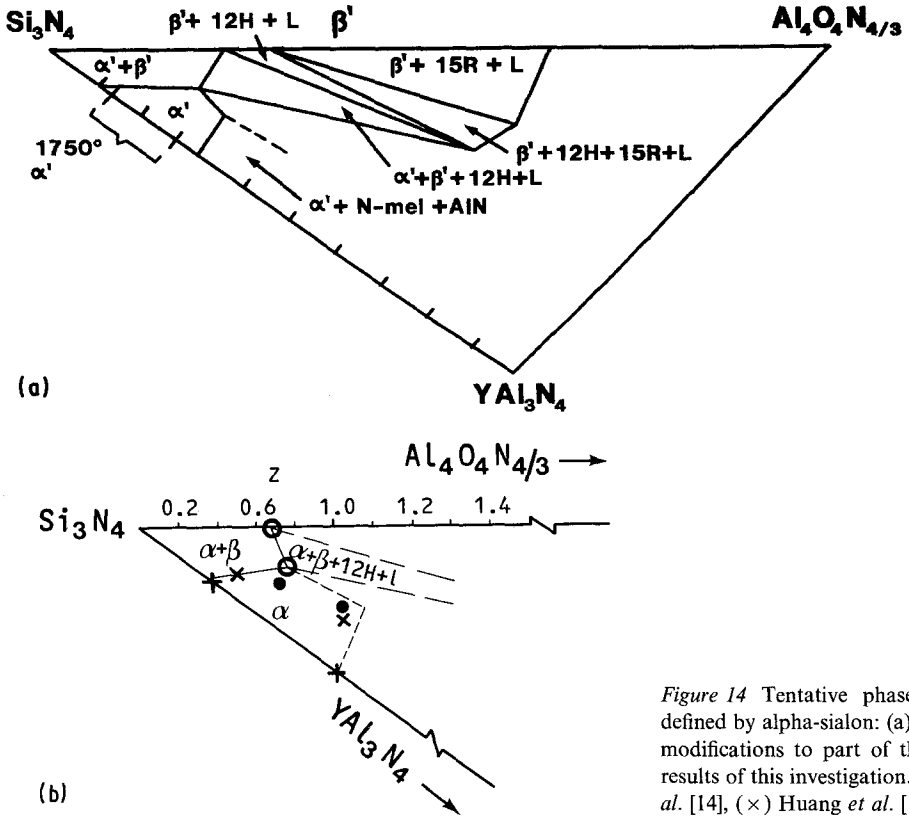

Figure 14 Tentative phase-relationship diagrams in the plane defined by alpha-sialon: (a) Suggestion of (a) Spacie *et al.* [14]; (b) modifications to part of the previous diagram suggested by the results of this investigation. (●) Hampshire *et al.* [4], (+) Spacie *et al.* [14], (×) Huang *et al.* [16], (○) own results.

In addition, impurities like calcium or magnesium in the raw materials, which might segregate to the glass phase and drastically reduce its viscosity, have a possibility of substituting into the alpha-sialon structure or the sialon polytype in Grade 3. Indeed, both Grades 2 and 3 perform much better than Grade 1 in high-speed metal-cutting performance tests using superalloy work pieces [21]. In these tests a very high temperature is generated at the interface between the cutting insert and the newly formed metal chip.

The thermal diffusivity behaviour is in agreement with the observations of Xi *et al.* [22] and Mitomo *et al.* [23]: it decreases as the amount of alpha-sialon increases. The decrease in thermal diffusivity is significant. It is known that crystallization of an amorphous grain-boundary phase, as has happened in Grade 3, will normally increase the thermal diffusivity of a sialon ceramic by some 10% [24]. This should mean that the temperature generated at the chip/cutting insert interface is greatest for Grade 3, and thus that its chemical wear and plastic deformation are greatest. However, this is not so and it can only be assumed that other factors, in particular the greater amount of an amorphous grain-boundary phase, are the reason for the poorer cutting performance of Grade 1.

The occurrence of iron silicide inclusions in Si_3N_4 materials is well known, and because of their detrimental effect upon mechanical properties [25] they should be avoided by the use of raw materials with low iron content. The occurrence of silicon carbide phases in contact with the silicides can be readily explained by the fact that iron enhances the decomposition of Si_3N_4 to silicon [25, 26]. As the sialon grades are sintered in graphite-lined furnaces the carbon pick-up that occurs results in the formation of SiC. The remaining silicon forms an iron silicide during cooling.

In Figs. 6 and 7 it is seen that both alpha- and beta-sialon phases contain unreacted cores of alpha- and beta-Si_3N_4 surrounded by the corresponding sialon highly alloyed with aluminium. It is very possible that the observation that all specimens contain a percentage of very large particles, especially marked for the beta-sialon phase, is due to these cores. The abnormal grain growth can possibly be caused by factors such as the mean alpha- and beta-grain size, their particle-size distribution and the alpha/beta ratio in the Si_3N_4 starting material. The occurrence of large beta-Si_3N_4 fragments seems to be particularly important in this respect. Experiments are in progress using different silicon nitrides to see what effect removal of the coarse particles in the sintered microstructure have on the cutting and mechanical properties of sialon ceramics. The aluminium-rich border surrounding the cores is presumably the result of having rather different liquid-phase compositions in the initial stages of liquid-phase formation, at low temperatures than that which occurs when most of the liquid phase forms at the sintering temperature. Experiments have been performed in which unreacted powder mixtures were heated in a thermal analyser, following the production sintering cycle, and have shown that the first sign of liquid-phase formation occurs at about 1600 K. This temperature is in fair agreement with the ternary eutectic observed in the Y_2O_3–Al_2O_3–SiO_2 system by Lewis and co-workers [13, 27].

Finally, a comparison of the XRD and EPMA results suggests that either of these techniques can be used in quality-control procedures as they are in agreement as to the composition of the alpha-sialon and beta-sialon phases. However, the XRD technique is to be preferred as it is much quicker than EPMA, and also indicates what other phases are present.

5. Conclusions

1. By increasing the AlN + Al_2O_3 content, precipitation of the alpha-sialon phase in a sialon ceramic occurs which increases the hardness, especially at temperatures close to those existing at the cutting edge (1000 to 1200° C). In grades containing an (alpha + beta)-sialon mixture it is concluded that the presence of a grain-boundary phase has little effect upon hardness. This is probably due either to a reduction in the total amount of grain-boundary phase compared to a beta-sialon only material, or due to a partial conversion of the glass phase to a crystalline phase.

2. Precipitation of alpha-sialon decreases thermal diffusivity, but despite this, cutting materials containing large amounts of alpha-sialon perform much better than those without. This is possibly due to a reduction in the amount of liquid phase formed as the alpha-sialon content increases.

3. The alpha- and beta-sialon crystals seem, in many cases, to have started to grow on nuclei of alpha- or beta-Si_3N_4, respectively, present in the starting material. Large fragments of beta-Si_3N_4 in the Si_3N_4 powder probably give rise to a dispersion of coarse beta-sialon rods in the sintered material.

Acknowledgement

AB Sandvik Hard Materials are thanked for permission to publish this article.

References

1. K. H. JACK, *Metals Technol.* **9** (1982) 297.
2. G. PETZOW and J. LORENZ, in "Ceramic Science at present and in future" edited by S. Somiya (Uchida Rokakuho, Tokyo, Japan, 1981) p. 1.
3. C. CHATFIELD and H. NORSTRÖM, *J. Amer. Ceram. Soc.* **66** (1983) C-168.
4. S. HAMPSHIRE, H. K. PARK, D. P. THOMPSON and K. H. JACK, *Nature* **274** (1978) 880.
5. F. IZUMI, M. MITOMO and Y. BANDO, *J. Mater. Sci.* **19** (1984) 3115.
6. H. M. JENNINGS, *ibid.* **18** (1983) 951.
7. D. P. THOMPSON, in Proceedings of NATO-ASI, "Nitrogen Ceramics", edited by F. Riley (Noordof, Leyden, The Netherlands, 1977) p. 219.
8. G. SING, P. KORGUL, D. P. THOMPSON and A. HENDRY, in Proceedings of 12th International Congress of Crystallography, Ottawa, 1981 (International Union of Crystallography, Copenhagen) p. C-179.
9. E. M. TRENT, "Metal Cutting" (Butterworths, London, 1977) pp. 31–138.
10. G. R. ANSTIS, P. CHANTIKUL, B. R. LAWN and D. B. MARSHALL, *J. Amer. Ceram. Soc.* **64** (1981) 533.
11. R. E. TAYLOR and K. D. MAGLIC, in "Compendium of Thermophysical Property Measurements", Vol. 1, edited by K. D. Maglic (Plenum, New York, 1984) p. 256.
12. F. F. LANGE, *Ceram. Bull.* **62** (1983) 1369.
13. M. H. LEWIS and R. J. LUMBY, *Powder Metall.* **26** (1983) 73.
14. C. J. SPACIE, N. S. JAMEEL, D. P. THOMPSON and K. H. JACK, Journées d'etudes sur les nitrures, no. 6, St. Etienne, September 1984.
15. H. K. PARK, D. P. THOMPSON and K. H. JACK, *Sci. Ceram.* **10** (1980) 251.
16. ZHEN-KUN HUANG, P. GREIL and G. PETZOW, *J. Amer. Ceram. Soc.* **66** (1983) C-96.
17. K. H. JACK, in "Progress in Nitrogen Ceramics", edited by F. L. Riley (Martinus Nijhoff, The Hague, 1981) p. 45.
18. S. HAMPSHIRE, R. A. L. DREW and K. H. JACK, *J. Amer. Ceram. Soc.* **67** (1984) C-46.
19. D. CHAKRABORTY and J. MUKEJI, Second Report on "Evaluation of high temperature mechanical properties, fracture toughness and fracture mechanical parameters of Si_3N_4, SiC and sialon" (Central Glass and Ceramic Research Institute, Jadavpur, India, 1983).
20. J. E. MARION, A. G. EVANS, M. D. DRORY and D. R. CLARKE, *Acta Metall.* **31** (1983) 1445.
21. J. AUCOTE and S. R. FOSTER, *Met. Sci. Technol.*, to be published.
22. T. G. XI, O. T. CHEN, H. L. NI, F. Y. WU and T. S. YEN, *Trans. J. Br. Ceram. Soc.* **82** (1983) 175.
23. M. MITOMO, N. HIROSAKI and T. MITSUHASHI, *J. Mater. Sci. Lett.* **3** (1984) 915.
24. L. D. BENTSEN, D. P. H. HASSELMAN and T. Y. TIEN, *J. Amer. Ceram. Soc.* **67** (1984) C-85.
25. A. E. PASTO, *ibid.* **67** (1984) C-178.
26. D. R. MESSIER and E. J. DEQUIRE, *ibid.* **67** (1984) 602.
27. M. H. LEWIS, A. R. BHATTI, R. J. LUMBY and B. NORTH, *J. Mater. Sci.* **15** (1980) 103.

Received 29 March
and accepted 10 September 1985